Materials Science & Engineering B xxx (xxxx) 115918

Contents lists available at ScienceDirect

Materials Science & Engineering B

journal homepage: www.elsevier.com/locate/mseb

Ion irradiation of supported graphene: Defect formation and atmospheric doping

E.A. Kolesov [a, *], M.S. Tivanov [a], O.V. Korolik [a], V.A. Skuratov [b], O.O. Kapitanova [c, d], G.N. Panin [e]

[a] Faculty of Physics, Belarusian State University, 4 Nezavisimosti Av, 220030 Minsk, Belarus
[b] Joint Institute for Nuclear Research, Joliot-Curie 6, 141980 Dubna, Russia
[c] Faculty of Chemistry, Moscow State University, 1 Leninskie Gory, 119991 Moscow, Russia
[d] Center for Photonics and 2D Materials, Moscow Institute of Physics and Technology, 9 Institutskiy per, 141701 Dolgoprudny, Moscow Region, Russia
[e] Institute of Microelectronics Technology and High-Purity Materials of RAS, Institutskaya, 6, 142432 Chernogolovka, Russia

ARTICLE INFO

Keywords:
Graphene
Defects
Ion irradiation
Substrate
Adsorption
Doping

ABSTRACT

In this paper, we study structural and adsorption properties of graphene irradiated with 46 MeV Ar ions and 240 keV H ions on SiO_2/Si and copper substrates by micro-Raman spectroscopy. Graphene irradiated with H ions demonstrated evidence of both high and low defect density regions on a sub-micron scale. TRIM calculations showed that substrate was the dominant defect source with a contribution from about 55% for H ions in graphene on SiO_2/Si to 90% for Ar in graphene on SiO_2/Si. Charge carrier density analysis showed *p*-type adsorption doping saturating at $(0.48 \pm 0.08) \times 10^{13}$ cm^{-2} or $(0.45 \pm 0.09) \times 10^{13}$ cm^{-2} with a defect density of 1.5×10^{11} cm^{-2} or 1.2×10^{11} cm^{-2} for graphene on SiO_2/Si or copper, respectively; this was analyzed in the framework of physisorption and dissociative chemisorption. This study is useful towards the development of functionalization methods, molecular sensor design, and any graphene application requiring modification of this material by controlled defect introduction.

1. Introduction

Ion irradiation of graphene is a universal and convenient method for the controlled introduction of defects into the material structure. This method can be used to control the electrical, optical, catalytic, and other properties of graphene [1–3]. However, due to the fact that graphene is a monolayer, the probability of direct defect generation (through the nuclear collisions) can be rather small for certain ion types and energies [4]. At the same time, the substrate actively participates in the defect formation process in ion-irradiated graphene by means of a number of different mechanisms, including the substrate sputtering and the substrate recoil atoms reaching the graphene-substrate interface (boundary) with a non-zero energy [1–3,5–8]. Thus, the study of the relationship between defect formation in graphene under ion irradiation by the substrate-related mechanisms and directly by the incident ions will make it possible to increase the controllability of the process, obtaining the desired result by simply choosing combination "substrate - ion type / energy". Moreover, this will allow to exclude undesirable effects when graphene is irradiated when supported by a substrate.

The high sensitivity of graphene and its modifications to adsorbates makes this material promising for applications in selective catalysis, molecular and environmental sensors, medical applications, etc. [9]. Thereby, it is of current interest to study the effect of graphene structural modification through the introduction of defects on its adsorption properties. It is known that the atmospheric environment leads to spontaneous *p*-type doping of graphene due to the adsorption of H_2O and O_2 [10–15]. In this context, it is important to determine the basic properties of irradiated graphene adsorption doping under the atmospheric environment, in order to achieve better understanding of the relationship between the adsorption doping of graphene and its defect density, as well as to ensure the efficiency of graphene-based molecular sensor design.

Raman spectroscopy utilized in this work as a method to probe pristine and irradiated graphene structural and adsorption properties is a versatile non-destructive method for characterizing two-dimensional materials [16].

The purpose of the present work is to investigate structural and adsorption properties of ion-irradiated graphene by micro-Raman spectroscopy; this manuscript presents simultaneous study of both irradiation effects and adsorption effects, which is a convenient combination for studying the relationship between the mechanisms of defect formation in graphene under ion irradiation and adsorption doping of this

* Corresponding author at: Bobruiskaya str., 5, room 332, 220006 Minsk, Russia.
E-mail address: kolesov.bsu@gmail.com (E.A. Kolesov).

https://doi.org/10.1016/j.mseb.2022.115918
Received 14 March 2022; Received in revised form 22 July 2022; Accepted 27 July 2022
0921-5107/

material. The possibility of studying both of them within the same set of samples, along with the utilized methods, makes it possible to determine the limiting values for the adsorption doping saturation of graphene with defects, which are of both fundamental and practical importance. This study distinguishes the substrate effect either on defect formation or on adsorption separately, which allows to perform a deeper analysis into the reasons for the differences in data for different substrate cases.

2. Experimental

Graphene was synthesized by chemical vapor deposition on 99.999% pure Alfa Aesar copper foil substrate, 10 × 30 cm^2, 25 μm thick, pre-annealed at 1060 °C under 300 standard cubic centimeters per minute (sccm) hydrogen flow and 2,000 sccm argon flow at a pressure of less than 10^{-4} Torr for 1–2 h inside the reactor. Graphene growth was performed at 1020 °C with CH_4 flow of 40 sccm and hydrogen flow of 10 sccm; the cooling rate was described in detail elsewhere [17]. Graphene was transferred to commercially available SiO_2/Si (oxide thickness of 90 nm over a 500 μm Si wafer) and copper (25 μm thick) using PMMA-mediated method [18]. PMMA with a molecular weight of 996 000, dissolved in anisole, was spin-coated (3000 rpm, 1 min) on graphene supported by copper foil substrate; then, $(NH_4)_2S_2O_8$ aqueous solution (0.1 M) was used for copper etching, and water/isopropyl alcohol mixture was used in order to remove the etching products from graphene [19]. PMMA was removed by submerging the sample in glacial acetic acid (extra pure) [20] for 4 h. The resultant samples were identified as monolayer graphene by Raman spectroscopy (see Results and discussion section for more detail).

Graphene was irradiated by 46 MeV Ar ions with fluences of 10^9, 10^{11} and 10^{13} cm^{-2} at the IC100 cyclotron at the FLNR JINR in Dubna [21]. Ion beam homogeneity over the irradiated sample surface was controlled using beam scanning in the horizontal and vertical directions and was better than 5%. Graphene irradiation with 240 keV hydrogen ions was performed using ESU-2 horizontal electrostatic accelerator at the A.N.Sevchenko Scientific Research Institute, Belarusian State University, the fluence was of 5 × 10^{16} cm^{-2}. The irradiation conditions were configured, on one hand, to use typical light and heavy ions utilized in the irradiation of nanomaterials, and on the other – to activate a variety of damage mechanisms in order to broaden the spectrum of observed effects.

Raman spectra of the experimental samples were obtained using Nanofinder HE (LOTIS TII) confocal Raman spectrometer. To excite Raman radiation, a continuous-wave solid-state laser with a wavelength of 473 nm was used. Raman measurements were carried out using laser radiation power of 240–2400 μW, laser spot diameter was of 0.6 μm, the spectral resolution was better than 3 cm^{-1} (~2.3 cm^{-1} for G peak and ~1.0 cm^{-1} for 2D peak). Prior to the adsorption-related measurements, the samples were exposed to ambient air with a relative humidity ranging from 40% to 60% for at least one month. We did not find any evidence suggesting defected graphene degradation during 1 month exposure within the sensitivity of Raman measurements.

The substrate irradiation effects were simulated using the binary Monte Carlo method implemented in the SRIM/TRIM code [22]. Within the framework of this software, simulating the screened Coulomb ion-atom interaction, quantum–mechanical calculations of collision parameters are carried out taking into account the exchange and correlation interactions for the overlapping electron shells; besides, generation of electronic excitations and plasmons in the target is considered [22]. For the calculations, Monolayer Collision mode was used (calculation taking into account each collision without any approximations) with a statistics of 100,000 incident ions for a substrate layer with a thickness of at least 300 Å. Sputtering was described by the average sputtering yield and the average energy of the sputtered atoms.

It should be noted that within the framework of this study, the TRIM code was used exclusively to consider the irradiation effects associated with the substrate, in accordance with [3,5,8,23]. Calculation of defect formation directly in two-dimensional materials, including sputtering, *is not possible* using this software [4] due to the fact that the target is modeled as an amorphous matrix with a uniform mass distribution, and the effect of collisions is taken into account regardless of their density. To calculate the resultant defect density in graphene based on the modeling results, the defect yield / nuclear stopping dependencies from [8] were utilized.

3. Results and discussion

Typical Raman spectra of pristine and irradiated graphene on SiO_2/Si and Cu are presented in Fig. 1. Presence of graphene monolayer is confirmed by characteristic G and 2D features [16] and ratio of maximum intensities I_{2D}/I_G more than 1 for the pristine samples [24], 2D peak single-Lorentz profile, as well as values of 2D peak width of less than 35 cm^{-1} [16,25]. Along with the D peak not present in pristine samples, the specified features also confirm the absence of graphene oxide and small density of defects of less than 3 × 10^{10} cm^{-2} [16], which are related to trivial structural variations of pristine material. Irradiated graphene shows a pronounced D peak, which arises due to the presence of defects [26], its intensity increasing significantly for the irradiation with Ar (fluence of 10^{13} cm^{-2}) and H ions. The broadened and distorted Raman peak profiles for graphene irradiated with hydrogen ions along with a reduced 2D peak intensity indicate the presence of a significant number of defects after the ion treatment (the so-called “high defect density regime”, in which the average interdefect distance is less than ~5 nm) [26]. No evidence of irradiation-induced strain or rippling was observed in the experiments [16,27].

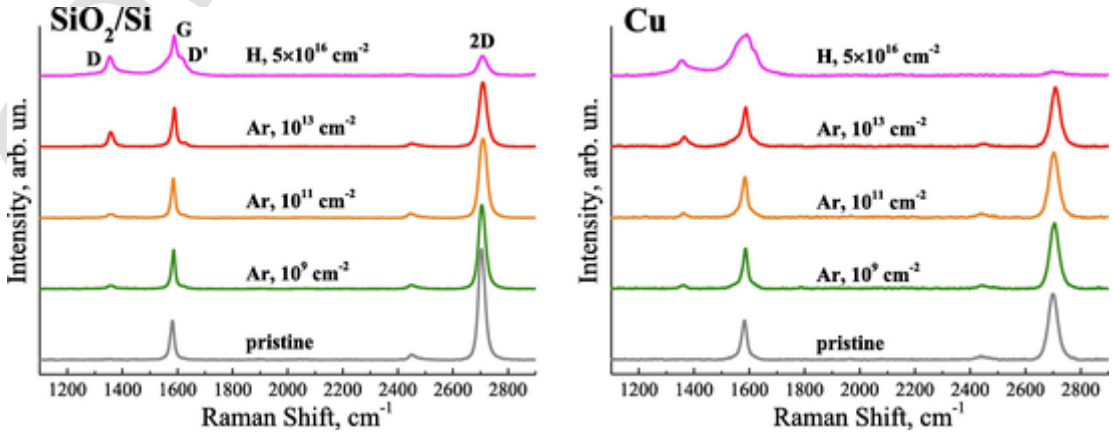

Fig. 1. Typical Raman spectra of pristine and irradiated graphene on SiO_2/Si and copper substrates.

While the I_D/I_G ratio is directly proportional to the defect density in the low defect density regime, this dependence reverses for stronger disordering of graphene crystal lattice, and the peaks broaden substantially [26]. At the same time, Raman spectra of H-irradiated graphene show only partial signs of high defect density regime, having distorted rather than clearly broadened peaks, and the 2D peak for graphene on SiO_2/Si is still substantially pronounced [26]. Therefore, the correct analysis here requires taking a closer look at the decomposition of the total signal into separate peaks by approximation, shown in Fig. 2.

As seen from Fig. 2, the approximation is in a very good agreement with the experimental points, showing the features typical for both low and high defect density regimes, i.e., one of the components distinguished by approximation corresponds to the direct part of the dependence from [26], and the other one – to the inverse part. Their superposition leads to the resultant distortion of the Raman peak profiles. This indicates the coexistence of high and low defect density regimes within the scale of 0.6 μm, i.e., the measurement is conducted in the area where regions with the interdefect distance both above and below ~ 5 nm are present. Since the hydrogen ion fluence of 5×10^{16} cm^{-2} corresponds to a resultant distance between the incident ion sites of ~0.03 nm, such spatial damage inhomogeneity can be explained by a low probability of a direct collision damage for a 2D material treated by ions [4] and the domination of substrate-induced defect formation [1–3,5–8] which should in principle depend on the substrate surface irregularities within a μm scale, natural for the substrate materials such as copper and SiO_2/Si.

In order to establish the defect density distribution over the sample surfaces, as well as to obtain statistics, Raman scanning of 20×20 μm^2 areas was performed. The I_D/I_G ratios calculated over the scanned areas for the pristine and Ar-irradiated graphene are presented in Fig. 3 (considering integrated peak areas instead of the intensities did not substantially affect the numerical results). As seen from the figure, a slightly pronounced uniform increase of the defect density is observed for graphene on both substrates under 10^9 and 10^{11} cm^{-2} fluence treatment, while in the case of 10^{13} cm^{-2} fluence, this parameter increases significantly. For graphene on copper substrate, more defects are introduced into graphene under 10^9 and 10^{11} cm^{-2} irradiation, than for SiO_2/Si; on the contrary, the map for the largest fluence shows a lower degree of material modification. The explanation of these effects requires additional calculations presented later in the text.

In addition to a near-uniform increase of a spatially homogeneous component, Fig. 3 shows localized defective points with a typical linear size less than the 1 μm scanning step, most likely generated during the transfer process by introducing strain which later gets released through the tearing of graphene [28]. Although no evidence of the polymer residue was observed around these points [29], the defects of such type can still appear due to the polymer-mediated graphene transfer as reported in [28]. While this can occur in the initially defect-free areas, the tearing is most probable at points where the defects in graphene are already present, having originated during the synthesis over the substrate defects. Upon irradiation, more defects are introduced in these areas, which seems quite natural. The absence of such points on part of the

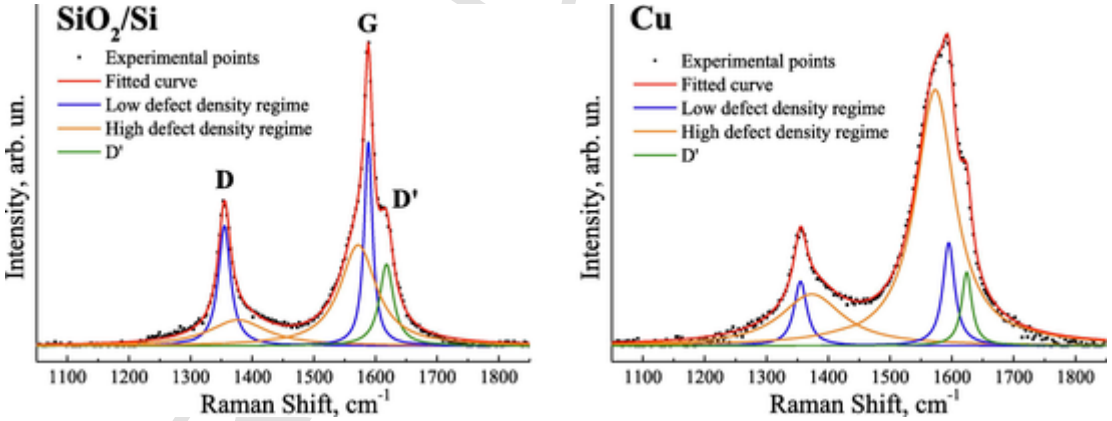

Fig. 2. G and D peak profiles for graphene irradiated with hydrogen ions on SiO_2/Si and copper substrates, decomposed into separate components. The D' peak is indicated separately as it can relate to both defect density regimes.

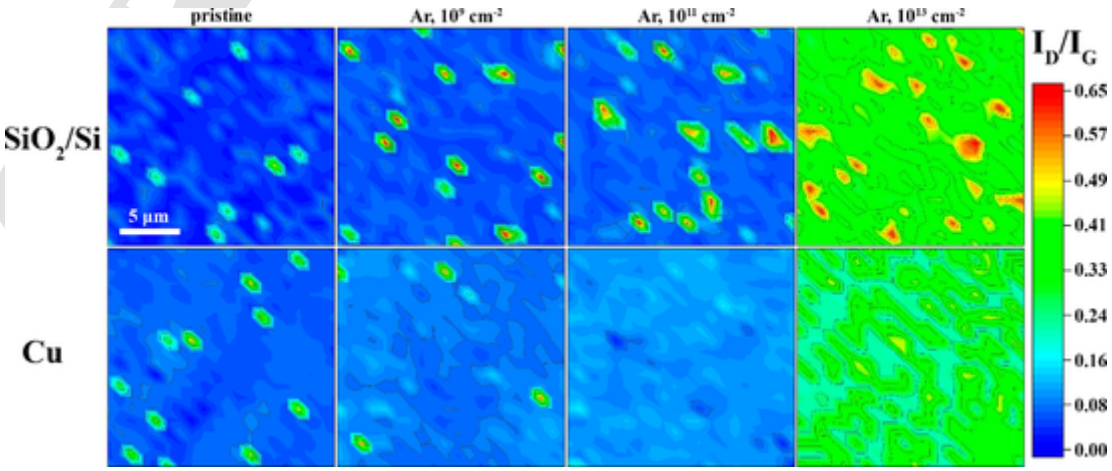

Fig. 3. 20×20 μm^2 Raman maps of I_D/I_G ratio representing the defect density for pristine and Ar-irradiated graphene on SiO_2/Si and copper substrates; scanning step of 1 μm.

maps indicates their uneven distribution over the sample surfaces within the given scale.

In the majority of the obtained pristine graphene Raman spectra, we did not observe D' peak which is known to depend on the defect type [30]. In the case of irradiated graphene, no pronounced $I_{D'}/I_D$ dependence on the ion fluence was observed; however, $I_{D'}/I_D$ values in all cases were in the range of 2.0–8.5, corresponding to the presence of vacancies and (or) grain boundaries [30].

Fig. 4 demonstrates I_D/I_G ratio maps for the samples irradiated with hydrogen ions, where the ratios for low and high defect density regimes are shown separately, as distinguished by the approximations. Again, a spatially uniform increase of the defect density is observed; for the copper substrate, irradiation leads to a stronger defect density increase, as evidenced by *greater* I_D/I_G values in the left map and *smaller* ones in the right one [26].

Table 1 presents the average defect density in pristine and irradiated graphene, calculated directly from I_D/I_G for all spectra obtained during the scanning by the well-known $n_D(I_D/I_G)$ expressions provided in [26]. Both defect density regimes were considered for graphene irradiated with hydrogen (the direct dependency for narrow components and the inverse one – for the broadened components [26]). Due to the absence of a distinguishable D peak in pristine graphene samples, the defect density for pristine graphene calculated from Raman basically illustrates the lower boundary of the measurable density range for a specific sample, which depends on several things including the noise level. It is seen from the table, that the average values generally follow the trends observed visually in Figs. 3 and 4: the defect density is not only ion type- and fluence-dependent, but also changes with the substrate material.

Due to varying defect density increase for graphene irradiation on different substrates under the same conditions, we can conclude that the substrate is actively involved in the defect formation process, which is in agreement with the literature [1–3,5–8]. Clarification of the specific substrate contribution requires additional calculations, where we focus primarily on substrate sputtering and electronic damage: the role of recoil atoms reaching the interface with a non-zero energy while remaining within the substrate is minimized for both 240 keV H and 46 MeV Ar in SiO_2/Si and Cu, according to comparative simulations performed in [31] for the estimation of relationship between different substrate-related mechanisms of defect formation in 2D materials under ion irradiation.

In order to obtain values of substrate sputtering yield Y_S and average sputtered atom energies ⟨E⟩, TRIM simulations were performed for the ion-substrate combinations studied in this work. Since TRIM is not directly applicable to 2D materials, the dependencies from [8] were thereafter used to calculate the resultant defect yield Y_D. The direct damage was calculated using stopping values of 8.62×10^{-3} keV/nm for Ar ions and 1.16×10^{-4} keV/nm for H ions (calculated for graphitic carbon in SRIM in accordance with [8], to obtain defect yields for graphene graphene defect yield / graphitic carbon stopping dependencies presented in the reference). The SRIM nuclear stopping in SiO_2 is 1.08×10^{-4} keV/nm for H and 8.55×10^{-3} keV/nm for Ar ions, in Cu – 2.74×10^{-4} keV/nm for H and 2.52×10^{-2} keV/nm for Ar ions. The calculation results for SiO_2/Si and copper substrates are presented in Table 2; as seen from the table, the substrate sputtering yield Y_S in the case of hydrogen irradiation is much smaller than that for Ar, which is natural considering the atomic mass difference. Comparing Y_S values for H in SiO_2/Si and copper can already explain smaller defect density for the former, seen in Fig. 4.

Based both on simulation results and on n_{Dexp} values calculated previously, we can estimate the relative contributions of direct collision defect generation, substrate sputtering and hot electron generation both in graphene and the substrate. The direct collisions and sputtering can be estimated simply in terms of Y_S and Y_D, then subtracted from n_{Dexp} in order to obtain density of defects related to hot electrons. Hot electron generation in the substrate can lead to graphene defect formation due to charge transfer only when electrons are generated in the immediate vicinity of the interface (for example, within the mean free path [31]); the electronic stopping represents the energy transferred to the target electronic sub-system, and the electronic yield is proportional to the electronic stopping. Therefore, distinguishing graphene and substrate hot electron effects in the basic approximation can be carried out through an assumption that it depends on the electronic stopping ratio for the corresponding materials. SRIM gives SiO_2 electronic stopping of

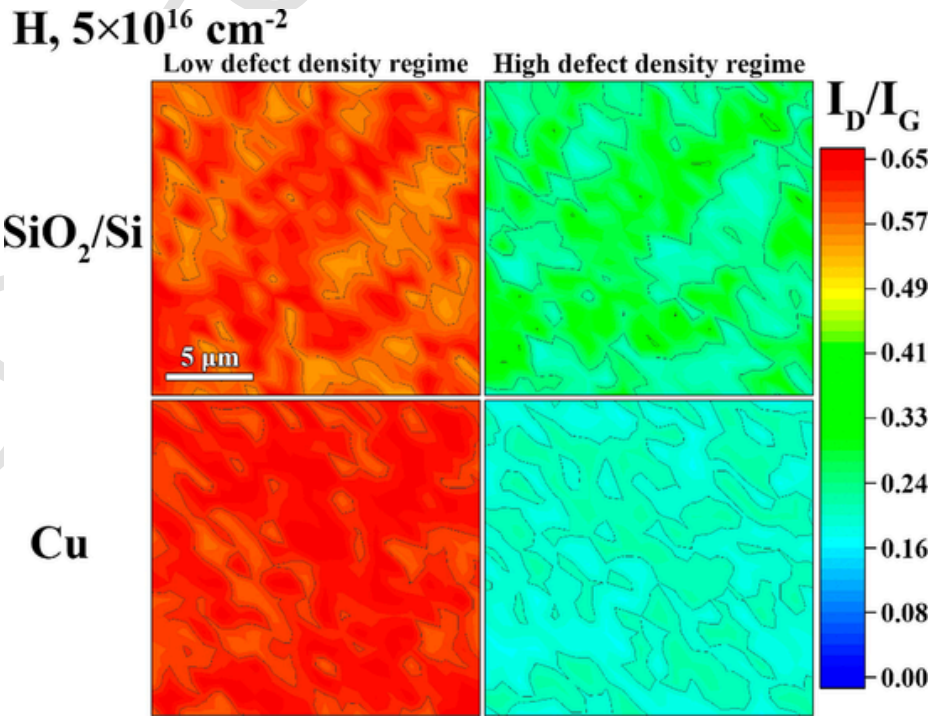

Fig. 4. 20 × 20 μm² Raman maps of I_D/I_G ratio representing the defect density for H-irradiated graphene on SiO_2/Si and copper substrates; scanning step of 1 μm.

Table 1
A summary of Raman spectral features for pristine and irradiated graphene on SiO_2/Si and copper substrates: average $\langle I_D/I_G \rangle$ values calculated over the Raman scans, and the corresponding average defect density in the scanned areas n_{Dexp}. In the case of hydrogen irradiation, the first and the second $\langle I_D/I_G \rangle$ values correspond to low and high defect density regimes, respectively.

Irradiation\parameter	SiO_2/Si		Cu	
	$\langle I_D/I_G \rangle$	n_{Dexp}, cm^{-2}	$\langle I_D/I_G \rangle$	n_{Dexp}, cm^{-2}
Pristine graphene	0.05	$\leq 1.7 \times 10^{10}$	0.08	$\leq 2.8 \times 10^{10}$
Ar (10^9 cm^{-2})	0.07	2.5×10^{10}	0.09	3.1×10^{10}
Ar (10^{11} cm^{-2})	0.08	2.9×10^{10}	0.10	3.6×10^{10}
Ar (10^{13} cm^{-2})	0.37	1.3×10^{11}	0.30	1.0×10^{11}
H (10^{16} cm^{-2})	0.59 0.26	2.6×10^{13}	0.62 0.20	3.7×10^{13}

Table 2
Simulation results for Ar and H irradiation of graphene supported by SiO_2/Si and copper, representing the substrate sputtering yield Y_S, ion energy or the average sputtered atom energy $< E >$, as well as the resultant defect yield (number of defects per ion or sputtered atom).

Irradiation	Damage source	Y_S, atoms/ion	$\langle E \rangle$, eV	Y_D, **defects/ion** (defects/atom)
Ar	Ar	–	4.6×10^7	**6.6×10^{-4}**
	Sputtered Si	0.0132	9.3×10^1	2.1×10^{-1}
	Sputtered O	0.0431	1.2×10^2	1.8×10^{-1}
	Sputtered Cu	0.1154	2.3×10^2	7.3×10^{-2}
H	H	–	2.4×10^5	**1.7×10^{-5}**
	Sputtered Si	0.0001	9.7×10^1	1.5×10^0
	Sputtered O	0.0004	1.7×10^1	6.3×10^{-1}
	Sputtered Cu	0.0014	3.7×10^1	5.8×10^{-1}

9.65×10^{-2} keV/nm for H ions and 4.76×10^0 keV/nm for Ar ions, and Cu electronic stopping of 1.83×10^{-1} keV/nm for H ions and 1.18×10^1 keV/nm for Ar ions.

The resultant contributions are given in Table 3. In order to obtain the most accurate results, n_{Dexp} values for the largest fluence of 10^{13} cm^{-2} were used, where total defect density increase differs significantly from ~10^{10} cm^{-2} intrinsic defect density. For all cases, the direct collision contribution is small, while the substrate is responsible for at least 55 % of the total damage and therefore can be considered the dominant defect source. The total hot electron contribution prevails for H irradiation, while the substrate sputtering is the most productive mechanism of defect formation in graphene in case of Ar ions. The contributions of hot electrons generated in graphene slightly exceed those in SiO_2/Si; the opposite is observed for Cu substrate.

We now move on to the studies of atmospheric adsorption on pristine and irradiated graphene. When exposed to atmosphere, graphene is known to endure gradual self-sustained hole doping, primarily by H_2O and O_2 adsorbates [10–15,32]. Presence of defects can obviously increase the energetic favourability of this process, leading to a stronger influence on the Raman spectra in terms of the charge carrier density (I_{2D}/I_G ratio, G peak position, 2D peak position) [32,33]. Due to a substantial number of defects introduced into graphene lattice during hydrogen irradiation, Raman spectra of these samples were not informative for the adsorption-related calculations. In order to confirm the presence of the adsorbates on pristine and Ar-irradiated graphene, we performed ~6 mW laser annealing according to the method presented in detail in [32]: Raman measurement at a point, then laser annealing, then a second measurement at the same point. The typical results of these sequences are given in Fig. 5. As seen, a near-constant I_D/I_G is preserved after the annealing, i.e., the defect density is not affected within the Raman spectroscopy sensitivity [26]. At the same time, notable changes of several Raman features can be observed, which include the I_{2D}/I_G ratio increase, G peak position decrease, as well as 2D peak shift All these changes are strongly indicative of hole density decrease in graphene due to the adsorbate removal from the sample surface during the annealing [32,33]; the smaller shift of the 2D peak is related to the fact that the dependency is more horizontal in the hole doping region, unlike in the case of negative Fermi level position below the Dirac point – this allows to unambiguously distinguish electron or hole doping of graphene from Raman spectroscopy [33].

One of the basic graphene Raman features depending on the charge carrier density is the I_{2D}/I_G ratio [33], which is given in Fig. 6 for the Ar-irradiated graphene on SiO_2/Si and copper. We note here that the intensity of the Raman signal may in principle depend on the degree of graphene crystal lattice disorder; however, we present these maps as part of a data set that also includes G and 2D peak positions, which are analyzed later in the text in more detail. In general, Fig. 6 demonstrates uniform softening of the I_{2D}/I_G ratio for greater fluences, which can indicate charge carrier density increase [33]; at the same time, considerably smaller values are seen for several points, which partially correspond to more defected areas observed in Fig. 3. Graphene on copper demonstrates smaller overall I_{2D}/I_G values, which in this case can relate to both stronger atmospheric doping typical for this substrate [15] and presence of the substrate-induced doping [34]. Metallic substrates are known to screen the electron–phonon coupling (EPC) in graphene [35], while the sensitivity of I_{2D}/I_G to the carrier density is due to the 2D peak intensity dependence on the EPC [33].

It was already mentioned in the previous paragraph that while the I_{2D}/I_G ratio is useful for illustrating carrier density distribution visually, it is not very convenient for obtaining quantitative results, since 2D peak intensity can become affected by graphene lattice destruction at higher defect densities. Therefore, we give another plot indicative of graphene adsorption doping in Fig. 7, presenting the statistics on G and 2D peak positions, which have individual, different and non-linear dependencies on the Fermi level position [33]. The figure clearly shows the distribution shift as the fluence changed, with the G peak shifting more notably, since the 2D peak is less sensitive to the carrier density in this range [33], and thus the plots for the latter related to different fluences mostly overlap.

The substrate influence on the distributions in Fig. 7 is manifested in a separation between the curves for graphene on SiO_2/Si and copper, more pronounced for 2D peak. The 2D peak position changes with the charge carrier density basically due to a dependence on graphene lattice constant [33], which is affected by doping and influences the phonon energy. Therefore, unlike the EPC-affected I_{2D}/I_G in Fig. 6, the higher 2D peak sensitivity to substrate material in this case has a different nature and is rather related to a stronger graphene-substrate interaction for copper, which leads to a more complex phonon interactions at the interface [36,37]. For G peak position, which depends on the carrier density due to being influenced by both lattice constant and the electron–phonon interactions, the stronger graphene-copper bonding and the EPC screening by Cu seem to partially counterbalance each

Table 3
The contribution of direct collision damage, substrate sputtering and hot electron generation to the total defect formation for graphene on SiO_2/Si and copper, irradiated with Ar and H ions.

Ions	Substrate	Direct collision contribution, %	Graphene hot electron contribution, %	Substrate sputtering contribution, %	Substrate hot electron contribution, %
Ar 46 MeV	SiO_2/Si	5.1	7.7	80.7	6.5
	Cu	6.6	3.0	84.2	6.2
H 240 keV	SiO_2/Si	0.7	43.8	15.5	40.0
	Cu	0.5	31.0	21.9	46.6

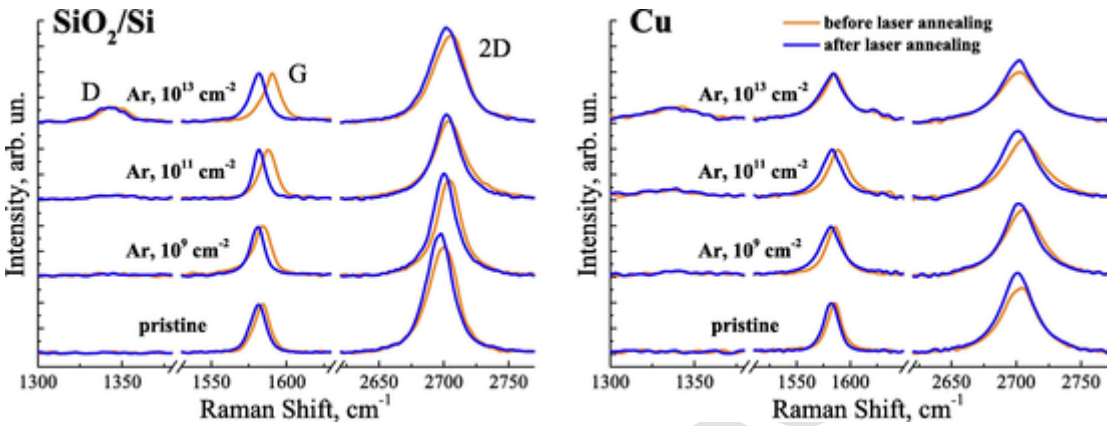

Fig. 5. Typical Raman spectra of pristine and Ar-irradiated graphene on SiO_2/Si and copper substrates before and after laser annealing.

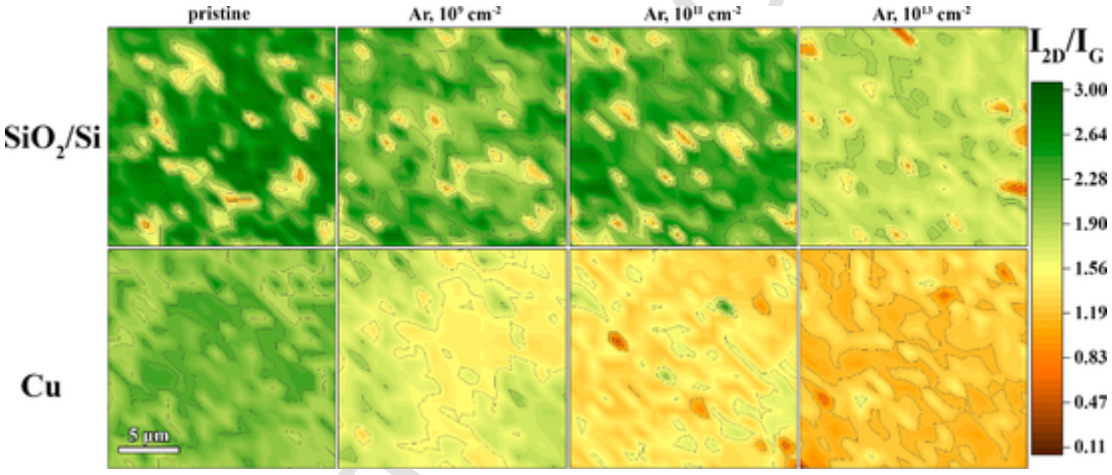

Fig. 6. 20 × 20 μm^2 Raman maps of I_{2D}/I_G ratio for pristine and Ar-irradiated graphene on SiO_2/Si and copper substrates; scanning step of 1 μm.

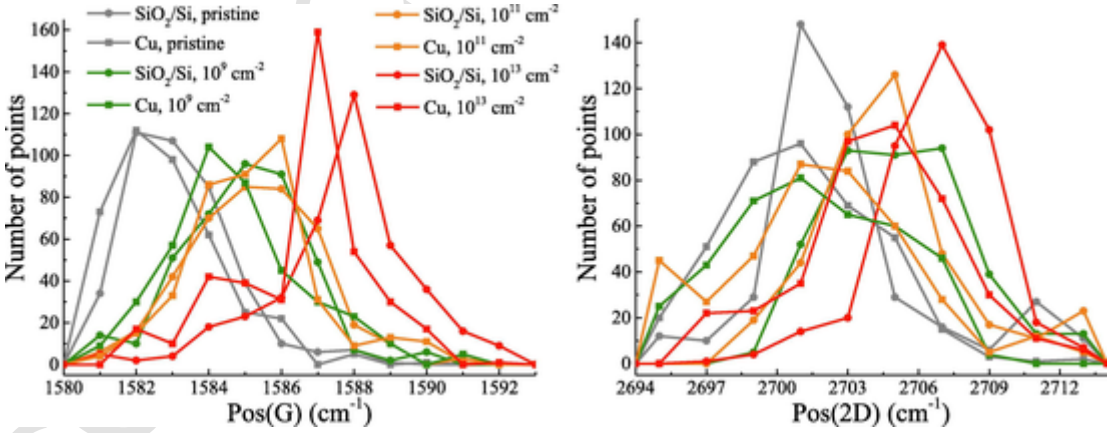

Fig. 7. Number of points corresponding to each G and 2D peak position for pristine and Ar-irradiated graphene on SiO_2/Si and copper substrates.

other, leading to mostly similar and overlapping distributions for different substrates.

The obtained set of the doping-dependent Raman features allow to calculate charge carrier density due to adsorption doping p [15,32,33], which was performed for pristine and Ar-irradiated material on SiO_2/Si and copper; simultaneously, the defect density was calculated for the corresponding points. Fig. 8 presents the obtained statistical plot, in which the semi-transparent symbols represent each point of the Raman scanning; it is evident from the figure that the adsorption doping tends to saturate as the defect density increases, which seems natural. It should be noted that while atmospheric doping of defect-free graphene occurs due to physical adsorption, introduction of vacancies provides sites for the dissociative chemical adsorption [38–40]. Therefore, Fig. 8 basically illustrates a shift from Van der Waals bonding domination at low defect densities to covalent bonding at the high ones [41].

The charge transfer from pristine graphene to adsorbate molecules is of 0.02e–0.03e per molecule in the case of O_2 and up to 0.01e–0.025e per molecule or aggregate for H_2O, all adsorption energies being below 1 eV [41–45]. In case of adsorption on a vacancy site, the charge transfer increases up to 0.6e and the adsorption energy for the dissociated molecules is above 3 eV [40,46,47]. Thus, the overall doping increase with the defectiveness in Fig. 8 is explained by two main reasons: (1)

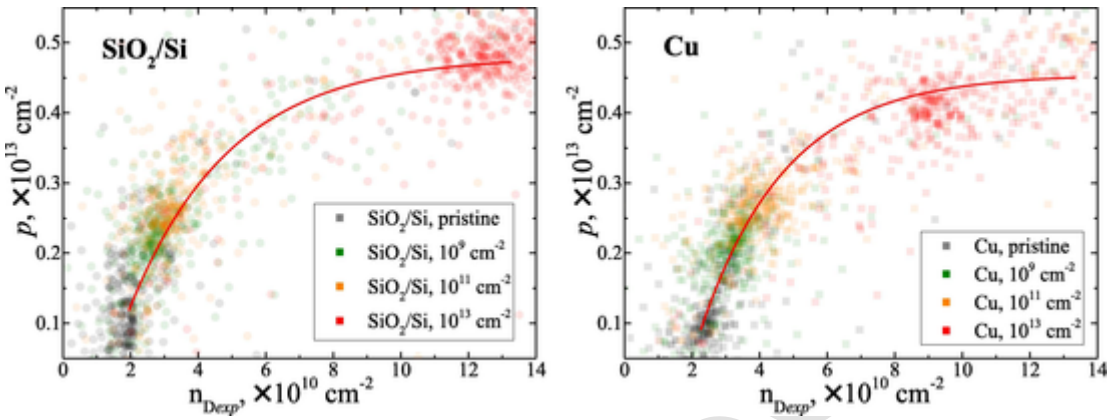

Fig. 8. Hole density depending on the defect density for pristine and Ar-irradiated graphene on SiO_2/Si and copper substrates. Solid lines visualize general dependency trends.

the atmospheric doping becomes more energetically favourable as the defect density increases, creating more sites for chemical adsorption, and therefore more adsorbates get attached to the sample surface; (2) more charge is transferred from graphene to the chemisorbed molecules comparing to the physisorbed ones. As the adsorbate density becomes higher, the positive charge of graphene increases, eventually hindering the acceptor adsorption. At the same time, graphene-adsorbate charge transfer depends on the adsorbed molecule orientation, so that the adsorbate can act as a donor [43–45]; the probability of these events is initially small but will obviously increase for a stronger electron deficiency, so that the donor adsorption will reduce both number of the adsorption sites and positive charge of graphene. Reaching the dynamic equilibrium between these processes provides the dependency saturation.

The asymptotic behavior of the plot in Fig. 8 allows to calculate maximum atmospheric adsorption doping of graphene p_{sat}, obtained as a result of defect introduction into the material. For graphene on SiO_2/Si substrate it shows the value of $p_{sat} = (0.48 \pm 0.08) \times 10^{13}$ cm^{-2}, reached within the error at $n_D^{sat} \sim 1.5 \times 10^{11}$ cm^{-2}. For graphene on copper, this parameter is estimated as $p_{sat} = (0.45 \pm 0.09) \times 10^{13}$ cm^{-2}, achieved at $n_D^{sat} \sim 1.2 \times 10^{11}$ cm^{-2} within the error. While the introduction of charge carriers of the same sign does reduce the physisorption doping probability [32], the initial *p*-type doping required for the absence of adsorption doping was previously estimated as 3.9×10^{13} cm^{-2} [32], which is more than 8 times larger than the calculated p_{sat}; therefore, we assume the density of physical adsorbates differs little from that for pristine graphene, although it may decrease slightly due to a decrease in the number of available physisorption sites.

Although the difference between p_{sat} for graphene on the two substrates is within the error, smaller value of n_D^{sat} for graphene on copper substrate means that in this case, the saturation occurs effectively earlier as the defectiveness increases. Stronger graphene-copper interaction with the energy of 0.72 J/m^2, as compared to 0.45 J/m^2 for SiO_2/Si [36], leads to smaller graphene-substrate distance for the former [48]. At the same time, graphene was shown to screen the Van der Waals interactions between the atmospheric adsorbates and the substrate only partially [49], which implies their stronger manifestation for Cu and therefore, stronger adsorption. Besides, copper substrate is known to screen the electron–electron interaction in graphene [35,50], causing Fermi velocity and Dirac point velocity to renormalize and distorting the Dirac cone [51], leading to possible charge carrier density increase [52].

The saturation values calculated in this work present additional limiting conditions to the studies of defected graphene enhanced adsorption [53–57], as well as adsorption-related electronic localization in defected graphene [58,59]. At the same time, these results show the defect density values, above which it is impractical to furtherly introduce defects to increase the adsorption properties [53–57]: the saturation of graphene adsorption doping with the increasing structural disorder means that after reaching n_D^{sat}, further defect introduction is not productive for the adsorptivity increase and will only destroy graphene lattice. The substrate affects the dependency in Fig. 8, and therefore may be utilized to modify graphene adsorption properties in the intermediate stages of reaching p_{sat}, while its role is not defining of p_{sat} value itself, which generally simplifies the control of this effect in terms of the molecular sensor design. At the same time, some influence on n_D^{sat} suggests considering other substrate materials providing a stronger/weaker interaction with graphene may be of interest. The results presented above are useful for the development of graphene functionalization methods [38], design of graphene-based sensors of various types [9,60], dosimetry [61], as well as for any nanoelectronics application requiring the modification of this material by a controlled defect introduction.

4. Conclusion

In this work, we performed Raman study of graphene irradiated with Ar ions (energy of 46 MeV) and H ions (energy of 240 keV) on SiO_2/Si and copper substrates. In the areas of 20 × 20 μm^2, uniform defect density increase was observed with the fluence at the scale of 0.6 μm scanning step. Raman spectra of graphene irradiated with H showed the evidence of both high and low defect density regimes, indicating that within the single measurement scale of 0.6 μm, regions with the interdefect distance both above and below ~5 nm are present. TRIM calculations showed that the substrate was the dominant defect source, its contribution to the total defect generation ranging from about 55 % in the case of H ions in graphene on SiO_2/Si to 90 % in the case of graphene on SiO_2/Si irradiated by Ar. That was provided by the substrate sputtering, which prevailed for Ar irradiation, or hot electrons generated in the substrate, which had significant effect in the case of H ions.

Charge carrier density analysis showed stronger *p*-type adsorption doping for larger defect density values, typical for more energetically favourable dissociative chemisorption over the vacancies. For graphene on SiO_2/Si or copper, this dependency saturated at $(0.48 \pm 0.08) \times 10^{13}$ cm^{-2} or $(0.45 \pm 0.09) \times 10^{13}$ cm^{-2} with a defect density of about 1.5×10^{11} cm^{-2} or 1.2×10^{11} cm^{-2}, respectively, which was explained by a competition of processes involving increasing graphene positive charge, and adsorption of molecules in orientations providing donor behaviour. This study is useful for the development of graphene functionalization methods, graphene-based molecular sensor design, as well as for any nanoelectronics application requiring the modification of this material by a controlled defect introduction.

Declaration of Competing Interest

The authors declare that they have no known competing financial interests or personal relationships that could have appeared to influence the work reported in this paper.

Acknowledgment

The reported study was funded by RFBR and BRFBR, project numbers 20-57-04010, 18-29-19120, 19-29-03050, in the framework of the state assignment of the Ministry of Science and Higher Education of the Russian Federation № 075-00920-20-00, as well as within the framework of the Belarus-JINR cooperation program.

Data Availability

The raw/processed data required to reproduce the images cannot be shared at this time as the data also forms part of an ongoing study. The experimental data required to reproduce the findings (synthesis, processing and measurement parameters), are available in the Experimental section.

References

[1] S. Zhao, J. Xue, Y. Wang, S. Yan, Effect of SiO_2 substrate on the irradiation-assisted manipulation of supported graphene: a molecular dynamics study, Nanotechnology 23 (2012) 285703.
[2] L. Madauß, O. Ochedowski, H. Lebius, B. Ban-d'Etat, C.H. Naylor, A.T. Charlie Johnson, J. Kotakoski, M. Schleberger, Defect engineering of single- and few-layer MoS_2 by swift heavy ion irradiation, 2D Mater. 4 (2017) 015034.
[3] S. Mathew, T.K. Chan, D. Zhan, K. Gopinadhan, A.-R. Barman, M.B.H. Breese, S. Dhar, Z.X. Shen, T. Venkatesan, J.T.L. Thong, The effect of layer number and substrate on the stability of graphene under MeV proton beam irradiation, Carbon 49 (5) (2011) 1720–1726.
[4] A.V. Krasheninnikov, K. Nordlund, Ion and electron irradiation-induced effects in nanostructured materials, J. Appl. Phys. 107 (2010) 071301.
[5] S. Kretschmer, M. Maslov, S. Ghaderzadeh, M. Ghorbani-Asl, G. Hlawacek, A.V. Krasheninnikov, Supported two-dimensional materials under ion irradiation: the substrate governs defect production, ACS Appl. Mater. Interfaces 10 (36) (2018) 30827–30836.
[6] G. Compagnini, F. Giannazzo, S. Sonde, V. Raineri, E. Rimini, Ion irradiation and defect formation in single layer graphene, Carbon 47 (14) (2009) 3201–3207.
[7] S. Mathew, T.K. Chan, D. Zhan, K. Gopinadhan, A.R. Barman, M.B.H. Breese, S. Dhar, Z.X. Shen, T. Venkatesan, J.T.L. Thong, Mega-electron-volt proton irradiation on supported and suspended graphene: a Raman spectroscopic layer dependent study, J. Appl. Phys. 110 (2011) 084309.
[8] W. Li, X. Wang, X. Zhang, S. Zhao, H. Duan, J. Xue, Mechanism of the defect formation in supported graphene by energetic heavy ion irradiation: the substrate effect, Sci. Rep. 5 (2015) 9935.
[9] Y. Shao, J. Wang, H. Wu, J. Liu, I. Aksay, Y. Lin, Graphene based electrochemical sensors and biosensors: a review, Electroanalysis 22 (10) (2010) 1027–1036.
[10] S. Ryu, L.i. Liu, S. Berciaud, Y.-J. Yu, H. Liu, P. Kim, G.W. Flynn, L.E. Brus, Atmospheric oxygen binding and hole doping in deformed graphene on a SiO2 substrate, Nano Lett. 10 (12) (2010) 4944–4951.
[11] L. Kong, A. Enders, T.S. Rahman, P.A. Dowben, Molecular adsorption on graphene, J. Phys. Cond. Matt. 26 (44) (2014) 443001, https://doi.org/10.1088/0953-8984/26/44/443001.
[12] Y. Yang, K. Brenner, R. Murali, The influence of atmosphere on electrical transport in graphene, Carbon 50 (5) (2012) 1727–1733.
[13] H. Pinto, A. Markevich, Electronic and electrochemical doping of graphene by surface adsorbates, Beilstein J. Nanotechnol. 5 (2014) 1842–1848.
[14] S.B. Kalkan, H. Aydın, D. Özkendir, C. Çelebi, The effect of adsorbates on the electrical stability of graphene studied by transient photocurrent spectroscopy, Appl. Phys. Lett. 112 (2018) 013103.
[15] E.A. Kolesov, M.S. Tivanov, O.V. Korolik, O.O. Kapitanova, X. Fu, H.D. Cho, T.W. Kang, G.N. Panin, The effect of atmospheric doping on pressure-dependent Raman scattering in supported graphene, Beilstein J. Nanotechnol. 9 (2018) 704–710.
[16] A.C. Ferrari, D.M. Basko, Raman spectroscopy as a versatile tool for studying the properties of graphene, Nat. Nanotech. 8 (4) (2013) 235–246.
[17] FETHULLAH Güneş, G.H. Han, KI.K. Kim, E.S. Kim, S.J. Chae, M.HO. Park, HAE.-KYUNG. Jeong, S.C. Lim, Y.H. Lee, Large-area graphene-based flexible transparent conducting films, Nano 4 (2) (2009) 83–90.
[18] X. Liang, B.A. Sperling, I. Calizo, G. Cheng, C.A. Hacker, Q. Zhang, Y. Obeng, K. Yan, H. Peng, Q. Li, X. Zhu, H. Yuan, A.R. Walker, Z. Liu, L.M. Peng, C.A. Richter, Toward clean and crackless transfer of graphene, ACS Nano 5 (2011) 9144.
[19] L. Gao, G.-X. Ni, Y. Liu, B. Liu, A.H. Castro Neto, K.P. Loh, Face-to-face transfer of wafer-scale graphene films, Nature 505 (2014) 190.
[20] M. Her, R. Beams, L. Novotny, Graphene transfer with reduced residue, Phys. Lett. A 377 (2013) 1455.
[21] B.N. Gikal, S.N. Dmitriev, G.G. Gul'bekyan, P.Y. Apel', V.V. Bashevoi, S.L. Bogomolov, O.N. Borisov, V.A. Buzmakov, I.A. Ivanenko, O.M. Ivanov, N.Y. Kazarinov, I.V. Kolesov, V.I. Mironov, A.I. Papash, S.V. Pashchenko, V.A. Skuratov, A.V. Tikhomirov, M.V. Khabarov, A.P. Cherevatenko, N.Y. Yazvitskii, Yazvitskii, IC-100 accelerator complex for scientific and applied research, Phys. Part. Nucl. Lett. 5 (1) (2008) 33–48.
[22] J.F. Ziegler, M.D. Ziegler, J.P. Biersack, SRIM – the stopping and range of ions in matter (2010), Nucl. Instr. Meth. Phys. Res. 268 (11–12) (2010) 1818–1823.
[23] E.A. Kolesov, M.S. Tivanov, O.V. Korolik, P. Yu Apel, V. A. Skuratov, A. Saad, I. V. Komissarov, Defect formation in supported graphene irradiated by accelerated xenon ions, J. Mat. Sci. Mater. Electr. 29 (4) (2018) 3296–3303.
[24] A.C. Ferrari, J.C. Meyer, V. Scardaci, C. Casiraghi, M. Lazzeri, F. Mauri, S. Piscanec, D. Jiang, K.S. Novoselov, S. Roth, A.K. Geim, Raman spectrum of graphene and graphene layers, Phys. Rev. Lett. 97 (2006) 187401.
[25] Y. Hao, Y. Wang, L. Wang, Z. Ni, Z. Wang, R. Wang, C.K. Koo, Z. Shen, J.T.L. Thong, Probing layer number and stacking order of few-layer graphene by Raman spectroscopy, Small 6 (2) (2010) 195–200.
[26] L.G. Cançado, A. Jorio, E.H.M. Ferreira, F. Stavale, C.A. Achete, R.B. Capaz, M.V.O. Moutinho, A. Lombardo, T.S. Kulmala, A.C. Ferrari, Quantifying defects in graphene via Raman spectroscopy at different excitation energies, Nano Lett. 11 (8) (2011) 3190–3196.
[27] D. Manno, L. Torrisi, L. Silipigni, A. Buccolieri, M. Cutroneo, A. Torrisi, L. Calcagnile, A. Serra, From GO to rGO: an analysis of the progressive rippling induced by energetic ion irradiation, Appl. Surf. Sci. 586 (2022) 152789.
[28] G. Cheng, I. Calizo, X. Liang, B.A. Sperling, A.C. Johnston-Peck, W. Li, J.E. Maslar, C.A. Richter, A.R. Hight Walker, Carbon scrolls from chemical vapor deposition grown graphene, Carbon 76 (2014) 257–265.
[29] E. Koo, S.-Y. Ju, Role of residual polymer on chemical vapor grown graphene by Raman spectroscopy, Carbon 86 (2015) 318–324.
[30] A. Eckmann, A. Felten, A. Mishchenko, L. Britnell, R. Krupke, K.S. Novoselov, C. Casiraghi, Probing the nature of defects in graphene by Raman spectroscopy, Nano Lett. 12 (8) (2012) 3925–3930.
[31] E.A. Kolesov, Choosing the Substrate for Ion Irradiation of Two-Dimensional Materials, Beilstein J. Nanotechnol. 10 (2019) 531–539.
[32] E.A. Kolesov, M.S. Tivanov, O.V. Korolik, E.Y. Kataev, X. Fu, O.O. Kapitanova, H.D. Cho, T.W. Kang, G.N. Panin, Atmospheric adsorption on pristine and nitrogen-doped graphene: doping-dependent, spatially selective, J. Phys. D: Appl. Phys. 53 (2020) 045302.
[33] R. Beams, L.G. Cançado, L. Novotny, Raman characterization of defects and dopants in graphene, J. Phys. Cond. Matt. 27 (2015) 083002.
[34] S. Ulstrup, M. Bianchi, R. Hatch, D. Guan, A. Baraldi, D. Alfe, L. Hornekær, P. Hofmann, High-temperature behavior of supported graphene: electron-phonon coupling and substrate-induced doping, Phys. Rev. B 93 (2016) 239901.
[35] D.A. Siegel, C. Hwang, A.V. Fedorov, A. Lanzara, Electron–phonon coupling and intrinsic bandgap in highly-screened graphene, N. J. Phys. 14 (2012) 095006.
[36] Y. He, W.F. Chen, W.B. Yu, G. Ouyang, G.W. Yang, Anomalous interface adhesion of graphene membrane, Sci. Rep. 3 (2013) 2660.
[37] E.A. Kolesov, M.S. Tivanov, O.V. Korolik, O.O. Kapitanova, H.D. Cho, T.W. Kang, G.N. Panin, Phonon anharmonicities in supported graphene, Carbon 141 (2019) 190–197.
[38] M. Oubal, S. Picaud, M.T. Rayez, J.C. Rayez, Adsorption of atmospheric oxidants at divacancy sites of graphene: a DFT study, Comput. Theor. Chem. 1016 (2013) 22–27.
[39] Y. You, J. Deng, X. Tan, N. Gorjizadeh, M. Yoshimura, S.C. Smith, V. Sahajwalla, R.K. Joshi, On the mechanism of gas adsorption for pristine, defective and functionalized graphene, Phys. Chem. Chem. Phys. 19 (8) (2017) 6051–6056.
[40] Q. Zhou, Y. Yong, X. Su, W. Ju, Z. Fu, X. Li, Adsorption behavior of O2 on vacancy-defected graphene with transition-metal dopants: a theoretical study, Int. J. Modern Phys. B 32 (27) (2018) 1850304, https://doi.org/10.1142/S0217979218503046.
[41] D.W. Boukhvalov, V.Y. Osipov, A.I. Shames, K. Takai, T. Hayashi, T. Enoki, Charge transfer and weak bonding between molecular oxygen and graphene zigzag edges at low temperatures, Carbon 107 (2016) 800–810.
[42] P. Giannozzi, R. Car, G. Scoles, Oxygen adsorption on graphite and nanotubes, J. Chem. Phys. 118 (2003) 1003.
[43] R.R.Q. Freitas, R. Rivelino, F.d.B. Mota, C.M.C. de Castilho, DFT studies of the interactions of a graphene layer with small water aggregates, J. Phys. Chem. A 115 (44) (2011) 12348–12356.
[44] O. Leenaerts, B. Partoens, F.M. Peeters, Adsorption of H2O, NH3, CO, NO2, and NO on graphene: a first-principles study, Phys. Rev. B 77 (2008) 125416.
[45] J.G. Brandenburg, A. Zen, M. Fitzner, B. Ramberger, G. Kresse, T. Tsatsoulis, A. Grüneis, A. Michaelides, D. Alfè, Physisorption of water on graphene: subchemical accuracy from many-body electronic structure methods, J. Phys. Chem. Lett. 10 (2019) 358–368.
[46] I.A. Pašti, A. Jovanović, A.S. Dobrota, S.V. Mentus, B. Johanssonde, N.V. Skorodumova, Atomic adsorption on graphene with a single vacancy: systematic DFT study through the periodic table of elements, Phys. Chem. Chem. Phys. 20 (2018) 858–865.
[47] P. Błoński, M. Otyepka, First-principles study of the mechanism of wettability transition of defective graphene, Nanotechnology 28 (6) (2017) 064003, https://doi.org/10.1088/1361-6528/aa53c5.
[48] O. Frank, J. Vejpravova, V. Holy, L. Kavan, M. Kalbac, Interaction between graphene and copper substrate: the role of lattice orientation, Carbon 68 (2014) 440–451.
[49] F. Presel, A. Gijón, E.R. Hernández, P. Lacovig, S. Lizzit, D. Alfè, A. Baraldi, Translucency of graphene to van der waals forces applies to atoms/molecules with different polar character, ACS Nano 13 (10) (2019) 12230–12241.
[50] M. Endlich, A. Molina-Sánchez, L. Wirtz, J. Kröger, Screening of electron-phonon

coupling in graphene on Ir(111), Phys. Rev. B 88 (2013) 205403.
[51] D.A. Siegel, W. Regan, A.V. Fedorov, A. Zettl, A. Lanzara, Charge-carrier screening in single-layer graphene, Phys. Rev. Lett. 110 (2013) 146802.
[52] J. Li, L.Z. Tan, K. Zou, A.A. Stabile, D.J. Seiwell, K. Watanabe, T. Taniguchi, S.G. Louie, J. Zhu, Effective mass in bilayer graphene at low carrier densities: the role of potential disorder and electron-electron interaction, Phys. Rev. B 94 (2016) 161406.
[53] D.J. Buckley, N.C.G. Black, E.G. Castanon, C. Melios, M. Hardman, O. Kazakova, Frontiers of graphene and 2D material-based gas sensors for environmental monitoring, 2D Materials 7 (2020) 032002.
[54] X. Jia, H. Zhang, Z. Zhang, L. An, Effect of doping and vacancy defects on the adsorption of CO on graphene, Mater. Chem. Phys. 249 (2020) 123114.
[55] X. Zhu, Y. Xu, Z. Cheng, Y. Wang, Z. Lu, G. Zhang, First principles study of atmospheric pollutants adsorption on non-defect and monatomic defect graphene, Diam. Rel. Mater. 112 (2021) 108252.
[56] C. Yu, Q. Liu, Z. He, X. Gao, E. Wu, J. Guo, C. Zhou, Z. Feng, Epitaxial graphene gas sensors on SiC substrate with high sensitivity, J. Semicond. 41 (2020) 032101.
[57] X. Gao, Q.u. Zhou, J. Wang, L. Xu, W. Zeng, Performance of Intrinsic and modified graphene for the adsorption of H2S and CH4: A DFT study, Nanomaterials 10 (2) (2020) 299, https://doi.org/10.3390/nano10020299.
[58] X. Zhu, K. Liu, Z. Lu, Y. Xu, S. Qi, G. Zhang, Effect of oxygen atoms on graphene: adsorption and doping, Physica E 117 (2020) 113827.
[59] N. Dimakis, I. Salas, L. Gonzalez, O. Vadodaria, K. Ruiz, M.I. Bhatti, Li and Na adsorption on graphene and graphene oxide examined by density functional theory, quantum theory of atoms in molecules, and electron localization function, Molecules 24 (2019) 754.
[60] L. Torrisi, L. Silipigni, G. Salvato, Graphene oxide/Cu junction as relative humidity sensor, J. Mater. Sci. Mater. Electr. 31 (14) (2020) 11001–11009.
[61] L. Torrisi, M. Cutroneo, D. Manno, A. Serra, A. Torrisi, L. Silipigni, Proton beam dosimetry based on the graphene oxide reduction and Raman spectroscopy, Vacuum 201 (2022) 111113.